Transient Cavitation by Quick Closing Pincers

[1]Francisco A. Godínez*; [1]Margarita Navarrete; [2]Oscar Chávez; [1]Enrique Guzmán

[1]Universidad Nacional Autónoma de México, Instituto de Ingeniería, Cd Mx, México, [2]Instituto Tecnológico de Chihuahua, Chihuahua, México

Abstract

A mechanical device that mimics the snapping-claw mechanism of alpheid shrimps was developed to study experimentally transient cavitation. The apparatus consists of a pair of clamps (jaws), each with an inner contour that conforms to a half-Venturi geometry. One of the jaws is rigidly attached between two optically transparent parallel plates (forming a socket) and the other one works on a pivot. The clamps are mounted in such a way that when they close a Venturi tube-like with open and closed ends is formed. For the experiments, the device was immerse a few centimeters under tap water at lab conditions. The pivoting jaw was locked into an open position; then, its rapid closing was triggered mechanically and was driven by the contraction of rubber bands. High-speed video was used to capture the characteristics of the flow induced by the sudden relative motion between clamps. A water jet formed along with a variety of cavitation structures, such as cloud shedding, vapor lobes, travelling vortex rings, and bubble clouds were revealed. The developed technique could be an inexpensive alternative to test the performance of different Venturi geometries in cavitation regimes without the need for pipes, valves, tanks, and pumps typically used in experiments with hydraulic circuits.

Keywords: transient cavitation; Venturi tube; snapping-claw; cavitation structures

1. Introduction

Snapping shrimps (Family Alpheidae) possess a claw that can grow to be half the size of their entire body [1]. When this claw is closed rapidly, a cavitation front forms and collapses to produce a loud snap [2] with energy over a broad range of frequencies ranging from a few hundred hertz to 200 kHz [3]. The majority of studies to characterize this snap sound have been conducted with live animals and in their natural habitat. Nevertheless, greater control, repeatability and scalability may be attained through the use of artificial devices to emulate the claw geometry and its fast closing mechanism, in order to understand and clarify the phenomena associated with the emission of the snap sound. In this sense, Hess et al. [4] fabricated and tested an enlarged transparent model (which basically consists of a pivoting plunger and a socket) to reproduce the closure of the snapper claw and the flow generated by this process. Experiments were performed using both high-speed particle image velocimetry (HS-PIV) and flow visualization. During claw closure a channel-like cavity was formed between the plunger and the socket featuring a nozzle-type contour at the orifice. Hess's measurements revealed maximum flow velocities of 1 m/s in the nozzle with the formation of a vortex ring that grows in time. However, these velocities are too low to produce pressure drops below the vapor pressure of the used liquid (water-glycerine mixture) at lab conditions, and thus no cavitation process was observed. The aim of this paper was to design and test a mechanical device to produce transient cavitation in a repetitive and controlled way by mimicking the snapping-claw mechanism of alpheid shrimps. The proposed design closes the pivoting jaw in less than 9×10^{-3} s and is powerful enough to drive the formation of cavitating structures, as revealed by high-speed videography and image processing.

2. Mechanical device

The CAD model used for experiments is shown in figure (1a). It is worthy of note that the pair of walls (4) serve to shape the socket (3) and are made of transparent PMMA to facilitate flow visualization; additionally, they serve as support for the lower clamp (2), pivot (5), attachments (7), and mechanical trigger (8). Each one of the clamps have an inner contour that conforms to a half-Venturi geometry. The lower clamp (2) is rigidly attached between the two optically transparent parallel plates (4) (which in turn are fixed to corbel type supports), while the upper clamp (1) works on the pivot (5). When closing the pincers a Venturi tube-like with open and closed ends is formed. The violent closure of the clamps is achieved by the contraction of the set of rubber bands (6). Figure (1b) depicts the size of the Venturi tube formed between the socket walls and the clamps (1) and (2) when they are closed. It is important to note that the used Venturi geometry is not typical; in the present design, the cross section of the tube is rectangular as that used in some scrubbers [5] (see figure 1c). Besides, the converging section is larger than the diverging one and the

*Corresponding Author, Francisco Godínez: fgodinezr@gmail.com

throat is as large as the converging section. Despite these differences with traditional Venturi geometries, the present configuration allows the formation of a strong jet that moves beyond the outlet of the divergent section; the direction of this flow is indicated in figure (1b) with an arrow.

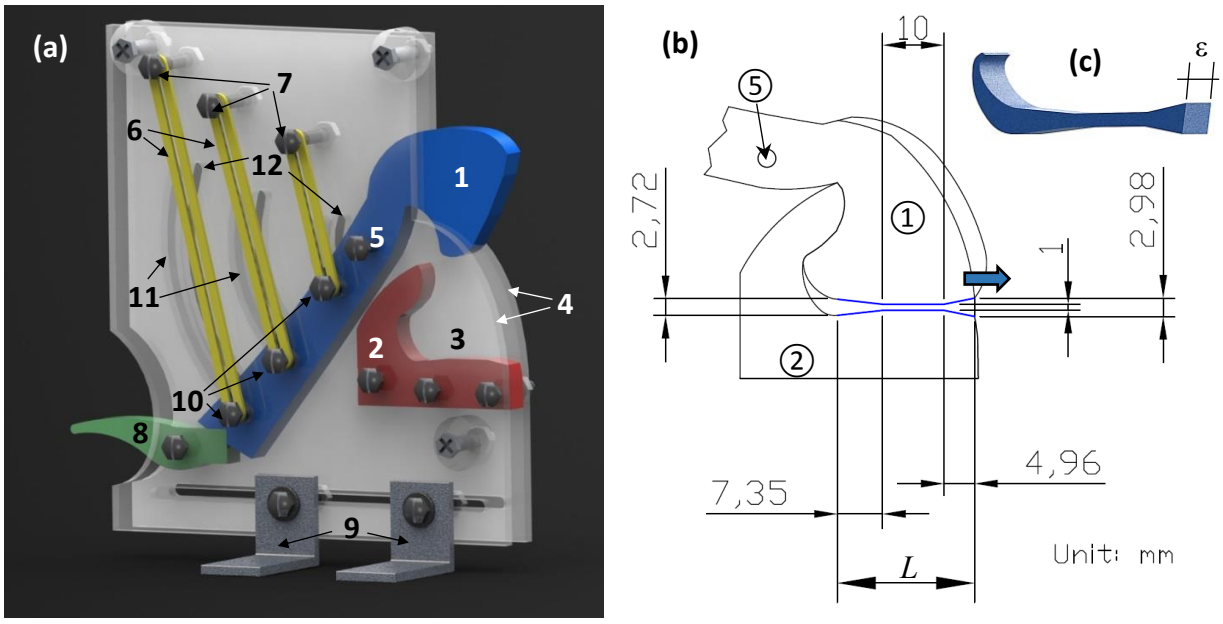

Figure 1 a) 3D CAD-model of the mechanical device to generate transient cavitation (open); 1) pivoting upper clamp, 2) fixed lower clamp, 3) socket, 4) walls, 5) pivot, 6) set of rubber bands, 7) set of band attachments, 8) mechanical trigger, 9) corbel type supports, 10) sliding bolts, and 11) curved sliding guides. b) Venturi tube-like geometry formed when clamps are totally closed. c) Three-dimensional scheme of the tube with rectangular cross-section formed when pincers are fully closed. The total length of the Venturi tube is L = 22.31 mm, and the distance between the walls (4) is ε = 5.8mm.

3. Experiments with high-speed video camera

3.1 Experimental setup

For the experiments, a rectangular tank (580 mm long, 500 mm wide and 270 mm deep) with transparent walls and filled with tap water at lab conditions (20° C, 77.86 kPa) was used. The upper clamp was locked into an open position (as seen in figure (1a)). The device was immersed in the tank 150 mm below the water level. The upper clamp was released by the mechanical trigger and its motion was recorded with a Phantom® v1212 high speed camera. To make the shots, the region of interest was illuminated with a 36,000 lumens lamp.

3.2 Dynamics and energetics of the closing process

Image processing and video analysis were applied to obtain the graph of the angular position of the upper clamp versus time (figure (3a)). The displacement ranges from the fully open position, when the clamp is mechanically released by the trigger (8), to the final position where the clamps are fully closed and the Venturi is formed. Figure (3b) represents the angular velocity developed by the upper clamp during the closing process. This curve was obtained by differentiating the curve of angular position of figure (3a). An acceleration region (i) is observed at the beginning of the closing process ($0 \le t/T \le 0.42$); region (ii) shows an almost constant rotation motion ($0.42 < t/T \le 0.7$); then a deceleration process is observed in the region (iii) ($0.7 < t/T \le 1$), which is slightly shorter than the region (i); finally, after the total closure, a series of bounces are visible in the region (iv) ($1 < t/T \le 1.29$). Such bounces are due to impact forces between the sliding bolts (10) and the uppermost part (12) of the curved sliding guides (11); see figure (1a).

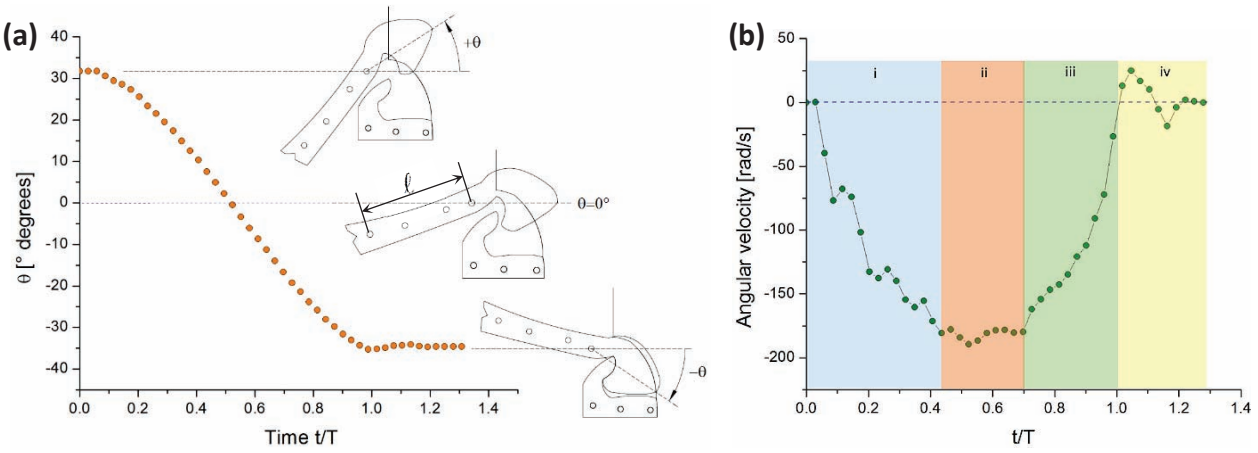

Figure 3 Time evolution of a) the angular position (data are averages of three experiments with SD of 0.6 [°degrees] or less), and b) the angular velocity of the upper clamp. In both graphs the horizontal axis is normalized with the total closure time, which is $T \approx 9$ ms.

Figure (4a) shows the curve of the torque (as a function of the angular position) that must be applied to open the upper clamp to its initial position; in terms of energy this represents around 3 J. By combining the angular velocity and torque data from figures (3b) and (4a), respectively, a power delivery curve is constructed. The average value of the power delivered is around 347 W (0.465 hp).

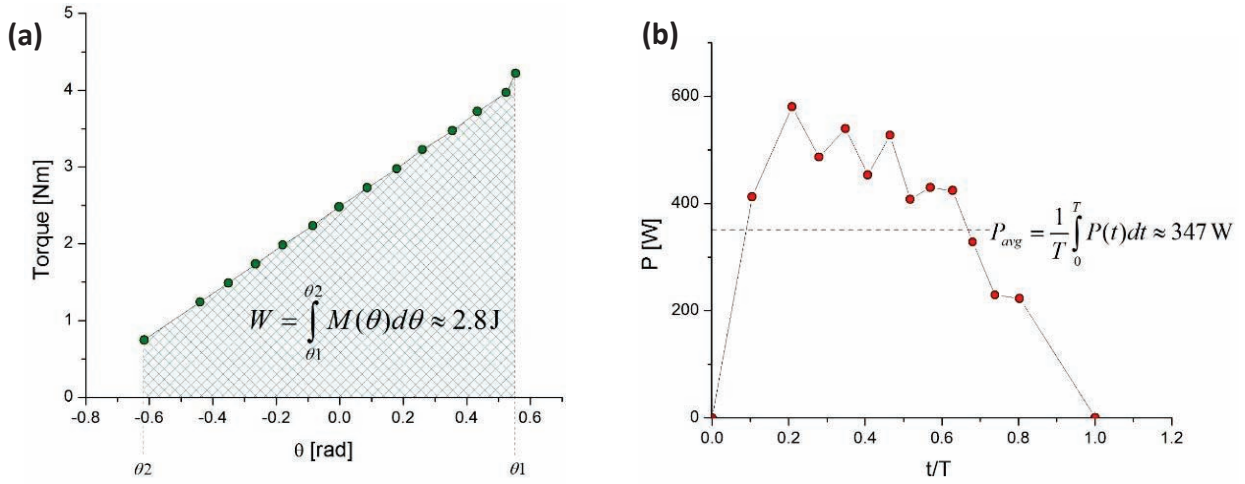

Figure 4 a) Torque (M) vs. angular position (θ); the points (solid symbols) were measured with a dynamometer considering a lever arm of length $\ell = 53mm$ (see figure (3a)). b) Power delivered by the pincers during the closing process.

3.3 Cavitation patterns and flow regimes

The high-speed photographic sequences of different cavitation patters and flow regimes were extracted from videos taken with a sampling frequency of 40,000 fps, and exposure time 10 μs. These were ordered chronologically from the moment in which the upper clamp is released, until a few instants after it closes completely.

3.3.1 No cavitation regime

Starting from t=0 s, when the upper clamp starts moving, and up to t ≈ 6.1 ms, no cavitating structures are observed.

3.3.2 Cavitation cloud shedding and vortex cavities

The motion of the upper clamp generates an incipient cavitating flow which is visible at t ≈ 6.125 ms, as indicated in the snapshot 1 of figure 5. This flow evolves and forms a cavitation cloud (snapshots 4, 5), and a series of vortices whose sizes increase as the upper clamp closes (snapshots 3, 6, 7). Bubble clouds originate in the leading-edge of the upper clamp (indicated in snapshot 2); from these clouds, a series of cavitating vortices are detached (snapshots 3, 6). This flow resembles in some sense the cavitating flow observed in hydrofoils and convergent divergent nozzles [6]. In the present case, however, the profile moves in relation to the static fluid and the flow is not periodic. Furthermore, an incipient cloud shedding is observed in the lower clamp (snapshot 5), a few moments later, tiny vortices are also formed and expelled into the free fluid (snapshots 7, 8).

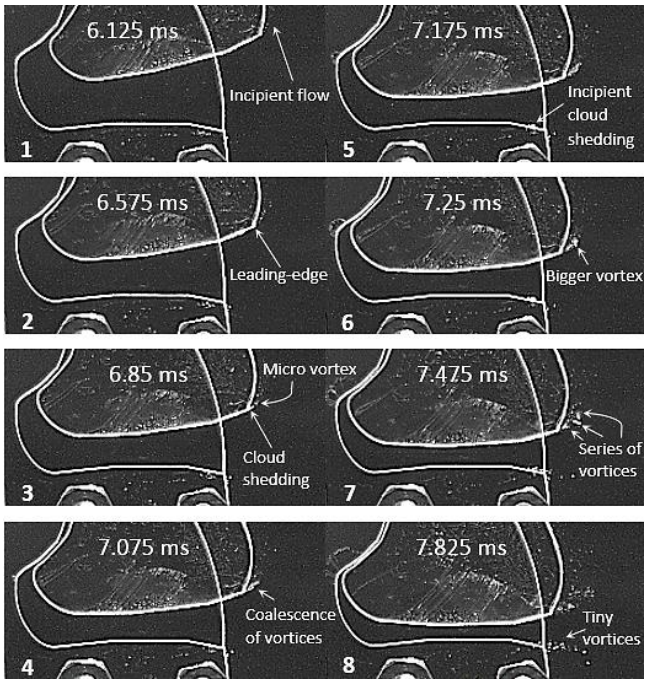

Figure 5 High-speed Photographic sequence of the cavitating flow induced by the pincers closing during the lapse 6.125 ≤ t ≤ 7.825 ms.

3.3.3 Vapor lobes, counter-rotating travelling vortex rings and cavitating sheet

Cavitation inception is observed at the lower edge of the throat, tiny vapor loves appear in both the upper and lower clamps (see snapshot 10 in fig.6). As time progresses, these lobes increase in size surrounding a water channel in the middle (snapshots 11, 12), something similar has been reported in [7]. Around the same time, some other cavitation structures appear. Photos 9 to 14 show the progressive growth of two counter-rotating travelling vortices in the free fluid; an upper vortex ring (indicated as V1) of small bubbles and a lower cavitating vortex ring (indicated as V2). A similar flow of two counter-rotating vortices (with no cavitation) at the exit of the diverging nozzle is experimentally observed in [4]. The inception and growth of a cavitating sheet in the upper wall of the throat is also observed from snapshot 13 onwards.

3.3.4 Vapor bubbles, cavitating vortex ring, bubble clouds and reverse flow

Photo 13 shows how the tips of the vapor lobes leave the divergent nozzle and come together to form a single lobe, as seen in photo 14. At the same time, millimetric vapor bubbles become visible at the upper clamp in the closed-convergent section. Their, growth, collapse (which release pressure waves), and rebound are visible from photo 14 onwards. Snapshots 15 to 17 show the process of formation of a leading vortex ring (indicated as V3). It is noticed that part of it begins to detach from the main lobe at 8.7 ms. At 8.75 ms, the vortex ring has practically detached from the single lobe, and moves with an average velocity of 14 m/s through the free fluid while it begins to collapse. Two

clouds of bubbles (indicated as CB1 and CB2) are observed at 8.9 ms; these are the product of the collapse and expansion of the vortex ring V3. Later on, the clouds CB1 and CB2 collapse and bounce to give rise to the single cloud CB3 observed at 9.35 ms; this cloud keeps moving while it disperses. Finally, at 9.775 ms, a cluster of tiny bubbles is observed, which still shows the basic structure of vortices V1, V2 and V3.

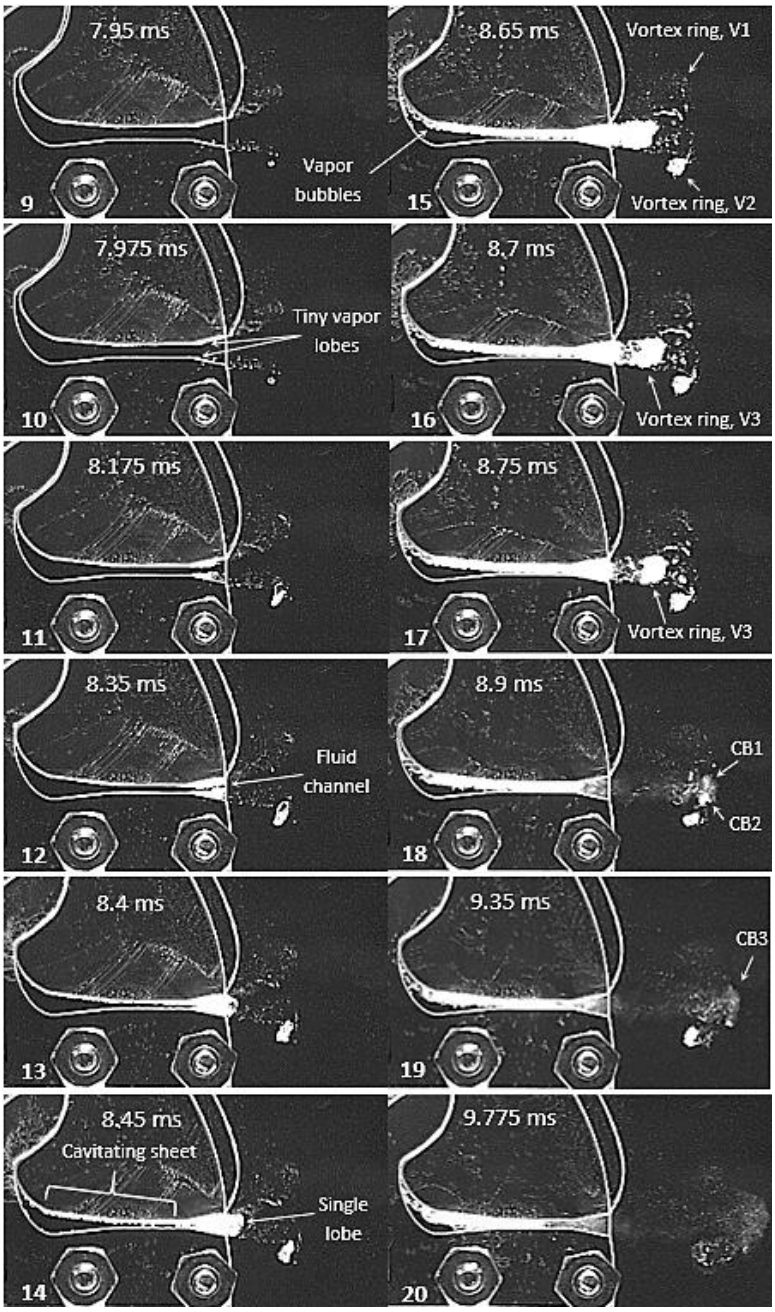

Figure 6 High-speed photographic sequence showing the cavitating flow induced by the motion of the pincers.

4. Dimensionless numbers of the induced flow

Table 1 compares the values of some dimensionless parameters that characterize the flow induced by the rapid closure of the shrimp claw and the pincers device. The average speed of the flow was measured from the exit of the throat to a few millimeters beyond the exit of the divergent section. The procedure consisted in following the motion of the tip of the upper cavitation lobe originated at the exit of the throat. Then the analysis from snapshots 9 to 14 (figure (6))

yields a value of $U \approx 14.5$ m/s. However, the flow velocity developed in the throat when the Venturi is formed (snapshots 9 to 11 in figure (6)) is greater than U. Respectively, the Cavitation, Reynolds and Strouhal numbers, were estimated with [4]: $Ca = \frac{p - p_v}{1/2\,\rho U^2}$, $\mathrm{Re} = \frac{U \cdot L}{\nu}$, $Sr = \frac{L}{T \cdot U}$. It is remarked that a very similar value of the Ca parameter was calculated for the shrimp claw and the pincers device; this value is less than 1, thus indicating the occurrence of cavitation [8] in both systems, a fact corroborated by our experiments.

	Alpheid shrimp	***Pincers***	***Scaling ratio***
Geometry	$L_0 \cong 1.41mm$	$L \cong 22.31mm$	$L / L_0 \cong 16$
Medium properties	$\nu_0 \cong 1cm^2 s^{-1}$	$\nu \cong 1cm^2 s^{-1}$	$\nu / \nu_0 \cong 1$
	$\rho_0 \cong 1g\,cm^3$	$\rho \cong 1g\,cm^3$	$\rho / \rho_0 \cong 1$
	$p_{v0} \cong 2333\,Pa$	$p_v \cong 2333\,Pa$	$p_v / p_{v0} \cong 1$
Closure time	$T_0 \cong 500\,\mu s$	$T_0 \cong 9ms$	$T / T_0 \cong 18$
Flow velocity	$U_0 \cong 17\,ms^{-1}$	$U \cong 14.5\,ms^{-1}$	$U / U_0 \cong 0.85$
Cavitation Nr.	$Ca_0 \cong 0.685$	$Ca \cong 0.732$	$Ca / Ca_0 \cong 1$
Reynolds Nr.	$\mathrm{Re}_0 \cong 24000$	$\mathrm{Re} \cong 323495$	$\mathrm{Re} / \mathrm{Re}_0 \cong 13.5$
Strouhal Nr.	$Sr_0 \cong 0.17$	$Sr \cong 0.17$	$Sr / Sr_0 \cong 1$

Table 1 Comparison between parameters of the shrimp claw and the pincers device, the data in the first column were taken from [4].

5. Conclusions

A mechanical device that emulates the snapping-claw mechanism of the pistol shrimp was designed and experimentally tested. The apparatus reproduces a variety of transient bubbly flow-regimes and cavitation-structures in a Venturi tube, and in the fluid near the open end of the tube. High-speed video recording proved to be insufficient to accurately establish the velocity of the water jet formed in the Venturi. Techniques such as PIV will be used in the future to precisely measure the velocity field. Furthermore, a photodiode and a hydrophone will be used to detect shock waves and luminescence, respectively. Both phenomena presumably result from the observed collapse and rebound of bubble clouds. The developed technique is simple, inexpensive, and shows great potential for testing the performance of different Venturi geometries. It proves particularly adequate to study cavitation regimes without the need for pipes, valves, tanks and pumps typically used in experiments with hydraulic circuits.

Acnowledgment: This research is funded by Programa de Apoyo a Proyectos de Investigación e Innovación Tecnológica PAPIIT de la UNAM. IN105117-2: Erosión por cavitación óptica, ultrasónica e hidrodinámica.

References

[1] Bohnenstiehl, D.R., Lillis, A., Eggleston, D.B. (2016). *The Curious Acoustic Behavior of Estuarine Snapping Shrimp: Temporal Patterns of Snapping Shrimp Sound in Sub-Tidal Oyster Reef Habitat.* PLoS ONE. 11(1).
[2] Versluis, M., Schmitz, B., Heydt von der, A., Lohse, D. (2000). *How snapping shrimp snap: Through cavitating bubbles.* Science. American Association for the Advancement of Science. 289.
[3] Cato, D.H., Bell, M.J. (1992) *Ultrasonic ambient noise in Australian shallow waters at frequencies up to 200 kHz*. Materials Research Laboratory, Australia; 1992 p. 27. Report No.: MRL-TR-91-23.
[4] Hess, D., Brücker, C., Hegner, F., Balmert, A., Bleckmann, H. (2013). *Vortex Formation with a Snapping Shrimp Claw.* PLoS ONE. 8(11).
[5] Overcamp, T. J. &. Bowen, S. R. (1983) *Effect of Throat Length and Diffuser Angle on Pressure Loss Across a Venturi Scrubber*, Journal of the Air Pollution Control Association. 33(6).
[6] Sato, K., Wada, Y., Noto, Y., Sugimoto, Y. (2010) *Reentrant Motion in Cloud Cavitation due to Cloud Collapse and Pressure Wave Propagation*. ASME. Fluids Engineering Division Summer Meeting, ASME 2010 3rd Joint US-European Fluids Engineering Summer Meeting: Volume 2, August 1–5, Montreal, Canada.
[7] Abdulaziz, A.M. (2014) *Performance and image analysis of a cavitating process in a small type venture*. Experimental Thermal and Fluid Science, 53.
[8] Gogate, P. R. & Pandit, A. B. (2000) *Engineering Design Methods for Cavitation Reactors II: Hydrodynamic Cavitation*. AIChE Journal. 46(8).